Hydrogen bonding in 2,6-bis(4-fluorophenyl)-3,5-dimethylpiperidin-4-one methanol solvate

T. Suresh,[I,II] V. Vijayakumar,[I] L. Jyothish Kumar,[I] S. Sarveswari*[I], Mukesh M. Jotani,[III] A. Otero-de-la-Roza,[IV] Yee Seng Tan[V] and Edward R. T. Tiekink*[V]

[I] VIT University, Centre for Organic and Medicinal Chemistry, Vellore, Tamil Nadu 632014, India

[II] Orchid Chemicals & Pharmaceuticals Ltd, R&D Centre, Chennai 600119, India

[III] Bhavan's Sheth R. A. College of Science, Department of Physics, Ahmedabad, Gujarat 380001, India

[IV] National Research Council of Canada, National Institute for Nanotechnology, 11421 Saskatchewan Drive, Edmonton, Alberta,

Canada T6G 2M9

[V] Sunway University, Research Centre for Crystalline Materials, Faculty of Science and Technology, 47500 Bandar Sunway, Selangor Darul Ehsan, Malaysia

Received; accepted

Keywords: Piperidin-4-one / conformation / DFT / crystal structure analysis / X-ray diffraction

Abstract. The crystal structure analysis of a 2,6-diaryl 4-piperidone derivative, isolated as a mono-methanol solvate, reveals that both the piperidone and the methanol molecule lie on a crystallographic mirror plane. A chair conformation is found for the piperidone ring with the aryl and methyl groups in equatorial positions. The most prominent feature of the molecular packing is the formation of supramolecular zigzag chains mediated by amine-N–H…O(methanol) and hydroxyl-O–H…N(amine) hydrogen bonds, i.e. the methanol molecule serves as a bridge between piperidone molecules. The molecular structure is compared with that determined in an unsolvated form and the gas-phase equilibrium structure, obtained using density-functional theory (DFT); differences relate, in the main, to the relative dispositions of the aryl rings. An analysis of the Hirshfeld surfaces of the experimental structures indicates very similar relative contributions with the notable exception being the contribution by O…H/H…O which at 13.7% in the methanol solvate is greater than 8.5% in the unsolvated form.

* Correspondence authors: sar.eswari@gmail.com (S.S.); edward.tiekink@gmail.com (E.R.T.T.)

Introduction

While the intermolecular interactions sustaining crystal structures are many and varied, hydrogen bonding remains as the mainstay of crystal engineering of the organic solid-state [1-4]. Being strong and highly directional, conventional hydrogen bonding can be exploited to rationally and reliably connect molecules into supramolecular aggregates as demonstrated, for example, in the burgeoning field of co-crystal formation [5, 6]. With the above in mind, it is clearly of fundamental interest when molecules with hydrogen bonding potential crystallise without forming hydrogen bonds, as these examples might provide insight into the role of other factors that determine the ultimate crystal structure(s) adopted by molecules. A notable example when conventional hydrogen bonds might be anticipated but are not observed is the crystal structure of 1,3-diazinane-2,4,5,6-tetrone (alloxan; Fig. 1a), which features two acidic amide-N–H atoms and four carbonyl groups. Rather than the formation of the what might be anticipated amide-N–H…O(carbonyl) hydrogen bonds, the most prominent intermolecular interactions, i.e. points of contact between molecules, are dipolar C=O···C=O contacts [7]. Such C=O···C=O contacts have been recognised for some time as being important in the molecular packing of both organic [8] and metalorganic crystal structures [9]. In the case of alloxan [7], global crystal packing considerations, correlated with the shape of the molecule, have been cited as being an overriding factor in determining the ultimate molecular packing in the crystal [10]. Herein, the crystal structure determination of 2,6-bis(4-fluorophenyl)-3,5-dimethylpiperidin-4-one (Fig. 1b), as its methanol solvate, is described. The structure of the organic molecule has been reported previously in an unsolvated form [11], and despite the presence of potential donor and acceptor hydrogen bonding sites, i.e. amine-N–H and carbonyl-C=O, conventional N–H…O hydrogen bonding was not observed in the molecular packing. The piperidin-4-one derivative has been by investigated by density-functional theory (DFT) methods, and the crystal structures of the solvated and unsolvated forms analysed by Hirshfeld surfaces.

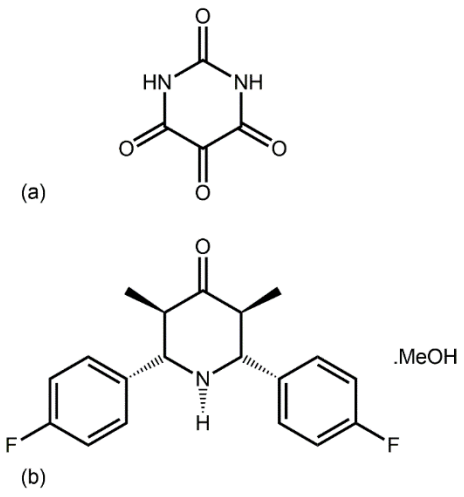

Fig. 1. Chemical structures of (a) 1,3-diazinane-2,4,5,6tetrone (alloxan), and (b) 2,6-bis(4-fluorophenyl)-3,5-dimethylpiperidin-4-one methanol solvate (**1**.MeOH).

Piperidin-4-one molecules are well known for their therapeutic applications and therefore great effort is directed toward the synthesis and characterisation of new derivatives. Specifically, piperidine derivatives are reported to exhibit anti-bacterial [12, 13] anti-fungal, central nervous system (CNS) stimulating, depressant and analgesic [14, 15], antitubercular [16], anti-cancer [17, 18] anti-oxidant and anticonvulsant [19] activities. The significant biological activities of piperidin-4-one derivatives are often associated with the aryl substituents at the positions on either side of the amine group [18, 20]. Thus, the pharmacological properties of potential piperidin-4-one drugs depend on the reactivity, stereochemistry and ring conformations of the compounds, especially for 2,6-diaryl 4-piperidones [21]. The title compound, **1**.MeOH, was investigated in continuation of earlier interest on piperidine derivatives [22-24].

Experimental

Instrumentation

All reagents used for the synthesis were purchased from Aldrich and used without further purification. The progress of the reaction was monitored by thin layer chromatography (TLC) using a mixture of 4:1 n-hexane and ethyl acetate as the eluent. The ^{1}H and $^{13}C\{^{1}H\}$ NMR (including the $^{1}H,^{1}H$ COSY) spectra were recorded in $CDCl_3$ solution on a Bruker-AVANCE III 400 MHz instrument with internal TMS as the standard. The melting point was determined on a Metler Toledo melting point apparatus by the open capillary tube method and was uncorrected. Powder X-ray diffraction (PXRD) data were recorded with a Bruker D8 Advance XRD system with Cu Kα1 radiation (λ = 1.5406 Å) in the 2θ range of 10.0 to 80.0° with a step size of 0.02°. The data acquired on the Bruker system were reformatted with PowDLL [25] into a form readable by X'Pert HighScore Plus [26] to enable a comparison between experimental and calculated (from the CIF) PXRD.

Synthesis and crystal growth

The synthesis of 2, 6-bis(4-fluorophenyl)-3,5-dimethylpiperidin-4-one was carried out by following the procedure available in the literature [27]. A mixture of diethylketone (0.86 g, 0.01 mole), fluorobenzaldehyde (2.48 g, 0.02 mole) and ammonium acetate (0.85g, 0.011 mole) in methanol was refluxed for about 0.5 h. The reaction mixture was then cooled to room temperature. The product was filtered and recrystallised from methanol; M. Pt: 388 K. NMR data: ^{1}H NMR (400 MHz): δ 7.44 (t, *J* = 8.0 Hz, 4H), 7.05 (t, *J* = 8.0 Hz, 4H), 3.62 (d, *J* = 8.0 Hz, 2H at C-2,6), 3.49 (s, 3H; CH_3 of methanol), 2.75 (t, *J* = 8.0 Hz, 2H at C-3,5), 2.05 (br s, 1H, NH), 1.40 (br s, 1H, -OH of methanol), 0.84 (s, 6H, CH_3 at C-3,5). ^{13}C-NMR (400 MHz): δ 186.48 (CO), 162.39 (*para*), 137.74 (*ipso*), 129.24 (*ortho*), 115.38 (*meta*), 68.02 (C-2 and

C-6), 52.11 (C-3 and C-5), 50.74 (methanol CH_3), 10. 41 (CH_3 at C-3 and C-5) ppm.

Crystal structure determination

Intensity data were measured at 100 K on an Agilent Technologies SuperNova Dual CCD with an Atlas detector fitted with Mo Kα radiation. Data processing and absorption correction were accomplished with CrysAlis PRO [28]. With the use of SHELXS-97 [29] and SHELXL-2014/7 [30] programs integrated into WinGX [31], the structure was solved by direct methods and refined on F^2 by full-matrix least-squares with anisotropic displacement parameters for all non-hydrogen atoms. The C-bound H atoms were placed on stereochemical grounds and refined in the riding model approximation with U_{iso} = 1.2-1.5U_{eq}(carrier atom). The O- and N-bound H atoms were refined with O–H = 0.84±0.01 and N–H = 0.88 ±0.01 Å, respectively, and with U_{iso} = 1.5U_{eq}(O) and U_{iso} = 1.2U_{eq}(N). A weighting scheme of the form $w = 1/[\sigma^2(F_o^2) + (0.038P)^2 + 1.350P]$ where $P = (F_o^2 + 2F_c^2)/3$ was employed. Unit cell data, X-ray data collection parameters, and details of the structure refinement are given in Table 1. The programs ORTEP-3 for Windows [31], PLATON [32], QMol [33] and DIAMOND [34] were also used in the analysis.

Table 1. Crystallographic data and refinement details for **1**.MeOH.[1]

Formula	$C_{19}H_{19}F_2NO$, CH_3OH
Formula weight	347.39
Crystal colour, habit	Colourless prism
Crystal size/mm	0.18 x 0.19 x 0.23
Crystal system	orthorhombic
Space group	*Pnma*
a/Å	9.2222(5)
b/Å	21.1828(10)
c/Å	9.0152(6)
V/Å^3	1761.14(17)
Z/*Z*′	4/1
D_c/g cm^{-3}	1.310
F(000)	736
μ(Mo*K*α)/mm^{-1}	0.098
Measured data	11036
θ range/°	3.2 – 27.5
Unique data	2070
R_{int}	0.020
Observed data ($I \geq 2.0\sigma(I)$)	1747
R, obs. data; all data	0.043; 0.051
R_w, obs. data; all data	0.104; 0.109

[1] Supplementary Material: Crystallographic data (excluding structure factors) for the structures reported in this paper have been deposited with the Cambridge Crystallographic Data Centre as supplementary publication no. CCDC-1426295. Copies of available material can be obtained free of charge, on application to CCDC, 12 Union Road, Cambridge CB2 1EZ, UK, (fax: +44-(0)1223-336033 or e-mail: deposit@ccdc.cam.ac.uk). The list of Fo/Fc-data

is available from the author up to one year after the publication has appeared.

Re-refinement of 1

At the suggestion of the anonymous reviewers of the original submission, a re-investigation of the location of the amine-H atom in the literature structure of **1** [11] was undertaken. This advice proved salutatory. In the literature refinement of **1**, the amine-H atom was placed in an "idealised" position with N–H1n = 0.86 Å. In the present study the acidic proton was removed and a difference Fourier map calculated. This revealed a plausible position for the amine-H atom. Unrestrained refinement of this position gave an N–H bond length of 0.91(17) and U_{iso} = 0.061(4) Å^2. In terms of hydrogen bonding, this new position gives an indication of a very weak hydrogen bond with the H1n···O separation in the putative amine-N–H···O(carbonyl) hydrogen bond of 2.593(15) Å and an angle at H1n of 156.9(13)º. However, the N–H separation is long for an sp^3-N–H bond. To be consistent with the refinement protocol for **1**.MeOH, the H1n atom in the new model for **1** was refined with N–H = 0.86 ±0.01 Å and with U_{iso} = 1.2U_{eq}(N). Details of the molecular packing of **1** are presented below. The new model for **1** gave rise to improvements in key indicators such as Rw (F^2; all data) = 0.164 cf. 0.212 for the original model, and $\rho_{max, min}$ = 0.22, 0.19 e Å^{-3} cf. 0.52, 0.43 e Å^{-3}.

Computational chemistry

The calculations were run using Density-Functional Theory (DFT) as implemented in the Gaussian code [35]. The B3LYP [36, 37] functional and the 6-31+G(2d,2p) basis set were employed to relax the geometries of several candidate conformers. The atomic charges were calculated using the Bader's QTAIM approach with the aimall program [38].

Results and discussion

Solution characterisation

To aid unambiguous assignment of the NMR data, a ^{1}H,^{1}H-COSY spectrum was recorded for **1**.MeOH, Fig. 2. The analysis showed that a doublet at δ 0.84 ppm, integrating for six protons, coupled with the triplet at δ 2.75 ppm (2H) enabling the assignment of the latter as being due to the methine protons at C-3 and C-5, i.e. nuclei carrying the methyl substituents. The signal at δ 2.75 ppm also coupled with a doublet at δ 3.62 ppm (2H) and so these were assigned as the methine protons at C-2 and C-6, i.e. bearing the aryl groups.

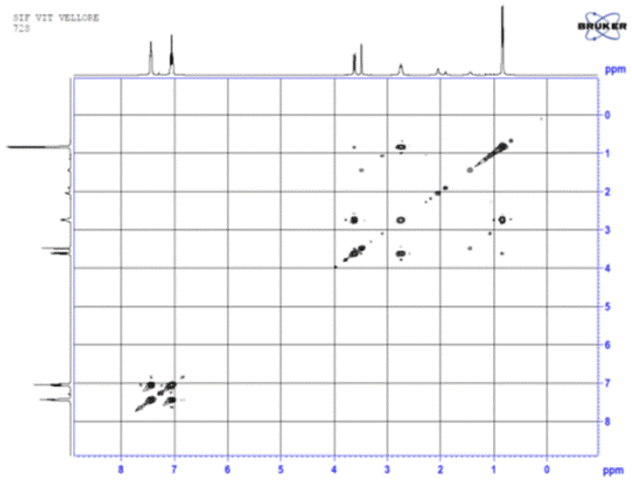

Fig. 2. The ^{1}H,^{1}H-COSY spectrum of **1**.MeOH, recorded in $CDCl_3$ solution.

The CH_3 proton of the solvent methanol molecule appeared as a singlet at δ 3.49 ppm and was coupled with the hydroxy proton of methanol which appeared as a broad singlet at δ 1.40 ppm; these were correlated in the ^{1}H,^{1}H-COSY spectrum. In the aromatic region, the signal at δ 7.44 ppm coupled with the signal at δ 7.05 ppm (4H). The downfield signal at δ 7.44 ppm was assigned to *meta* protons owing to their proximity to the electronegative fluorine atom at the *para* position enabling the assignment of the signal at δ 7.05 ppm to the *ortho* protons.

In the ^{13}C NMR spectrum, the extreme downfield signal at δ 186.48 ppm is readily assigned to the carbonyl carbon. Due to the presence of fluoride in the aryl ring, all the aryl carbons appeared as doublets. The aryl carbon at the *para* position, i.e. directly attached to fluoride, appeared as doublet at δ 162.39 ppm with $^{1}J_{CF}$ = 245 Hz. The signal at δ 137.74 ppm also appeared as doublet with $^{4}J_{CF}$ = 3 Hz, hence this was assigned to the *ipso* carbon. The doublets at δ 129.24 and 115.38 ppm, with $^{3}J_{CF}$ = 10 Hz and with $^{2}J_{CF}$ = 21 Hz, respectively, were assigned to *ortho* and *meta* nuclei, respectively. The downfield signal at δ 68.02 ppm was assigned to C-2 and C-6 (bearing aryl rings), whereas that at δ 52.11 ppm was assigned to C-3 and C-5 (having methyl substituents). The signal at δ 10.41 ppm is due to the methyl nuclei at C-3 and C-5. The methanol carbon appeared at δ 50.74 ppm. The above assignments, integration and coupling are entirely consistent with the structure shown in Fig. 1. The unambiguous structure determination of **1**.MeOH was established by single crystal X-ray crystallography.

Experimental crystal and molecular structures

The molecular structures comprising **1**.MeOH are shown in Fig. 3 and selected geometric parameters are collected in Table 2. The asymmetric unit comprises half a piperidone molecule and half a methanol molecule (crystallisation solvent), each of which lies on a crystallographic mirror plane.

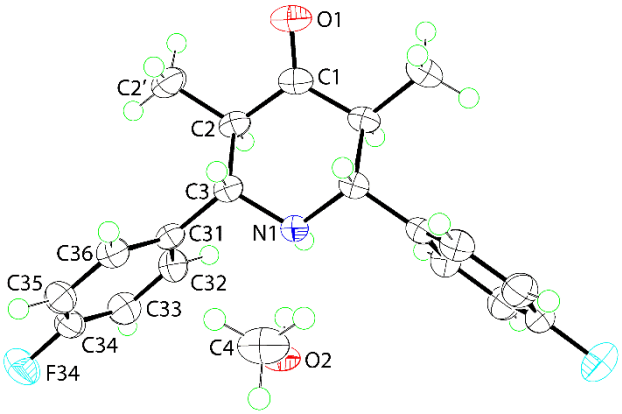

Fig. 3. Molecular structures in **1**.MeOH showing atom labelling scheme. The diagram is drawn at the 70% probability level. Unlabelled atoms are related by the symmetry operation: x, ½-y, z.

The piperidone ring has a chair conformation with the aryl and methyl groups occupying equatorial positions. In this description, all hydrogen atoms occupy axial positions with the amine-H atom being directed to the region between the aryl groups. Further discussion on the molecular structure of **1** in **1**.MeOH is found below under "Comparison of experimental **1**.MeOH and **1** with theoretical **1**".

The components of the crystal structure of **1**.MeOH are connected by a methanol-O–H···N(amine) hydrogen bond, Table 3. The dimeric aggregates are linked by amine-N–H···O(methanol) hydrogen bonds with the result that a zigzag supramolecular chain along the a-axis is formed, Fig. 4a; these chains are reinforced by aryl-C–H···O(methanol) interactions, Table 3. When viewed along the a-axis, it is evident that the connections between molecules are internal to the chain which appears to be tubular.

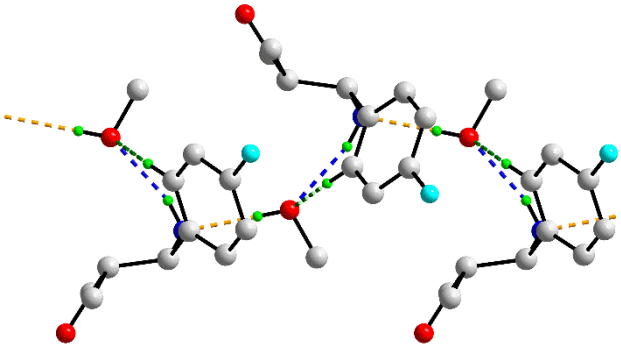

(a)

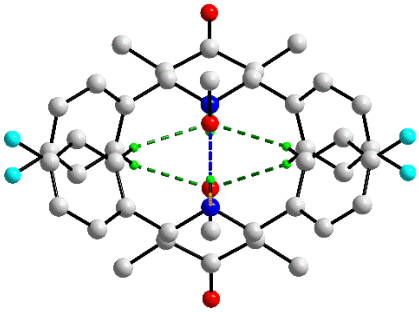

(b)

Fig. 4. Two views of the zigzag supramolecular chain along the a-axis in **1**.MeOH: (a) viewed normal to the mirror plane, and (b) viewed along the a-axis. The methanol-O-H…N(amine), amine-N-H…O(methanol) and aryl-C-H…O(methanol) interactions are shown as orange, blue and green dashed lines, respectively. Hydrogen atoms not participating in intermolecular contacts are omitted for reasons of clarity.

The supramolecular chains pack in the three-dimensional architecture with no specific interactions between them, at least based on the distance criteria in PLATON [32], Fig. 5. However, parallel rings (from symmetry, dihedral angle = ^{o}0) approach each other so that C35 atoms are in close proximity with the C35···C35^{i} separation being 3.302(2) Å; symmetry operation i: *-x*, *-y*, 1-*z*. This contact is discussed further below in the section describing the Hirshfeld surface analysis. In this description, there is no apparent role for the carbonyl-O and fluorine atoms in the directional supramolecular aggregation. The carbonyl-O atom sits in a pocket defined by hydrogen atoms. The two closest O···H contacts are intramolecular, i.e. 2 x O1…H2'3 = 2.61 Å, with the next closest being intermolecular, i.e. 2 x O1…H3^{ii} = 2.66 Å; symmetry operation ii: ½+*x*, ½-*y*, ½-*z*. These four hydrogen atoms define a trapezoidal plane about the carbonyl-O atom with the remaining contacts, shortest O···H separation = 2.89 Å (x 2), being above and below this plane. As for the O1 atom, the F1 atom is located in a pocket of hydrogen atoms, with the two closest contacts being intramolecular (F34…H33, H35 = 2.54 and 2.55 Å). The next closest contact is F34…H35^{iii} = 2.72 Å (symmetry operation iii: -½-*x*, *-y*, ½+*z*).

A comment is in order on the relative importance/strength of the interactions involving the carbonyl-O1 atom and the methine-H3 atom on the one hand, and between the methanol-O2 and aryl-H32 atoms on the other hand. All being equal, it might be anticipated that the O1···H3 interaction would be stronger than the O1···H32 contact as the methine-H3 atom would be expected to be more acidic, owing to its proximity to the amine-N1 atom, than the aryl-H32 atom. This is confirmed by the calculated pKa values of 45.0 (H3) and 46.9 (H32), as well as the Bader QTAIM charges, i.e. -0.0295 and zero, respectively. Therefore, it is assumed that steric pressures are responsible for the apparently weaker O1···H3 interactions.

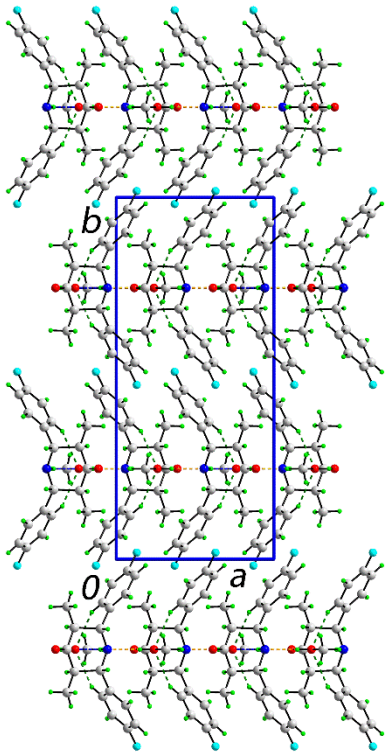

Fig. 5. A view in projection down the c-axis of the unit cell contents for **1**.MeOH. The methanol-O–H…N(amine), amine-N–H…O(methanol) and aryl-C–H…O(methanol) interactions are shown as orange, blue and green dashed lines, respectively.

Comparison of experimental 1.MeOH and 1 with theoretical 1

As mentioned in the Introduction, there is a precedent for the structure of **1**.MeOH, namely the unsolvated form **1** [11]. Salient geometric parameters for **1** in **1**.MeOH are collated in Table 3. The molecule of **1** was also subjected to energy-minimisation calculations. The energy-minimised structure is illustrated in the overlay diagram shown in Fig. 6 and geometric parameters for this are also included in Table 3. Several starting geometries were employed and it is noteworthy that the equilibrium molecular geometry is more stable, by 5.6 kcal/mol, than the conformer in which the nitrogen electron pair is aligned parallel to the aryl rings, possibly because of steric hindrance. Qualitatively, the molecular structures of the organic molecules in **1**.MeOH and energy-minimised **1** closely match each other, and differ from **1** observed in the unsolvated form [11].

Table 2. Summary of intermolecular interactions (A–H…B; Å, º) operating in the crystal structures of **1**.MeOH and **1** [11].[1]

A	H	B	A–H	H…B	A…B	A–H…B	Symmetry operation
1.MeOH							
O2	H2o	N1	0.845(12)	1.936(12)	2.781(2)	180(3)	*x*, *y*, *z*
N1	H1n	O2	0.877(15)	2.201(16)	3.056(2)	164.5(16)	½+x, ½-y, 1½-z
C32	H32	O2	0.95	2.49	3.3692(17)	153	½+x, ½-y, 1½-z
1							
N1	H1n	O1	0.875(11)	2.626(10)	3.4494(17)	157.1(13)	1+*x*, *y*, *z*
C11	H8	O1	0.93	2.49	3.400(3)	165	1-x, -y, 2-z
C18	H17	F1	0.93	2.54	3.197(3)	128	2-x, -y, 1-z
C12	H12c	Cg(C6-C11)	0.96	2.97	3.822(2)	149	-1+x, y, z

[1] Cg corresponds to the ring centroid of the specified atoms.

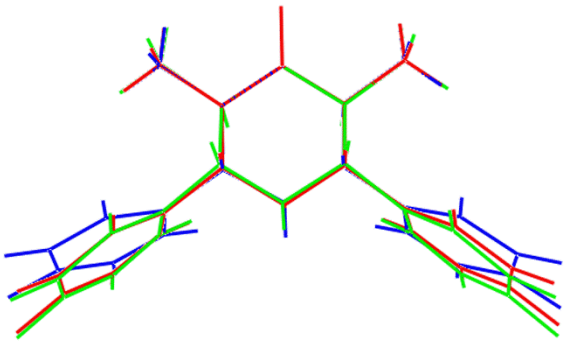

Fig. 6. Overlay diagram of the molecular structures of **1** in **1**.MeOH (red image), **1** (blue) and energy minimised **1** (green). The molecules have been overlapped so that the central rings are coincident.

From the data included in Table 3, it is apparent that there is agreement between key bond lengths and angles involving the heteroatoms in the ring with differences up to 4º in the C3–N1–C3^{i} angle between **1** in **1**.MeOH and the energy minimised **1**, and up to 5º in the N1–C3–C2 angles in **1** and energy minimised **1**. As might be expected, considerably more variability is noted in the torsion angle data highlighting the flexibility in the molecule, in particular pertaining to the relative dispositions of the aryl rings. In particular, differences up to 30º are noted in the N1–C3–C31–C32/C36 torsion angles. These adjustments allow for the different dihedral angles between the aryl rings which vary from a narrow 50.36(5)º in **1** to a wide 75.3º in the energy optimised structure of **1**.

Molecular packing in unsolvated 1

As the original report [11] of the crystal structure of **1** (unsolvated) contained only scant details of the supramolecular association sustaining the crystal structure, a more detailed description is now given. Geometric data for the identified intermolecular interactions are collected in Table 2. The key difference in the molecular packing of unsolvated **1** compared with **1**.MeOH is the participation of both the carbonyl-O and F atoms in directional intermolecular interactions. Conversely, no specific role for the amine-N–H atom is noted. Thus, aryl-C–H···O(carbonyl) interactions, occurring about a centre of inversion, lead to a 14-membered {…OC_5H}$_2$ synthon. These are connected by aryl-C–H···F interactions, also about a centre of inversion, leading to a 24-membered {…FC_5NC_4H}$_2$ synthon, as well as very weak methyl-C–H···π(aryl) contacts. This association has the result that supramolecular layers are formed in the ac-plane, Fig. 7. No directional intermolecular interactions between the layers are noted, Fig. 8.

Table 3. Summary of key geometric parameters (Å, º) for **1**.MeOH, **1** and energy minimised **1**.

Parameter	**1**.MeOH	**1**	Energy minimised **1**
C1–O1	1.214(2)	1.2094(18)	1.22
C3–N1	1.4756(16); 1.4756(16)	1.4605(17); 1.4623(17)	1.46; 1.46
C2–C1–O1	122.08(8); 122.08(8)	121.92(14); 122.12(14)	122.2; 122.2
C2–C1–C2^{i}	115.83(16)	115.96(12)	115.5
C3–N1–C3^{i}	111.55(15)	112.16(11)	115.9
N1–C3–C2	111.85(12); 111.85(12)	108.44(11); 112.11(11)	113.6; 113.7
O1–C1–C2–C3	-126.61(18); 126.61(18)	-130.06(15); 129.19(16)	-121.0; 121.0
O1–C1–C2–C2'	-2.6(2); 2.6(2)	-3.0(2); 3.0(2)	4.0; -4.0
N1–C3–C31–C32	-62.98(17); 62.98(17)	-50.00(16); 50.60(17)	-71.6; 71.6
N1–C3–C31–C36	115.64(15); -115.64(15)	135.29(13); -131.15(14)	106.6; -106.7
C2'–C2–C3–N1	-177.93(12); 177.93(12)	179.55(13); -178.92(14)	-174.9; 174.9
C2'–C2–C3–C31	58.47(16); -58.47(16)	56.42(17); -56.67(19)	59.9; -59.9
C2–C3–C31–C32	62.02(17); -62.02(17)	70.96(16); -70.17(17)	55.9; -56.0
C2–C3–C31–C36	-119.36(14); 119.36(14)	-103.76(15); 108.09(16)	-125.9; 125.8
(C31-C36)/(C31-C36)	70.22(4)	50.36(5)	75.3
(C2,C3,C2^{i},C3^{i})/(C31-C36)	75.17(7); 75.17(7)	81.38(6); 82.16(6)	71.5; 71.6
Symmetry operation i:	x, ½-y, z		

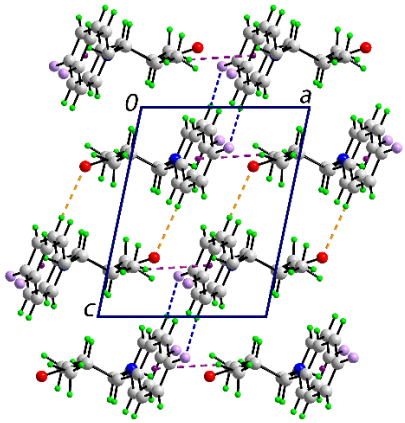

Fig. 7. A view of the supramolecular layer in **1** (unsolvated). The aryl-C–H···O(carbonyl), aryl-C–H···F and methyl-C–H···π(aryl) (largely obscured) interactions are shown as orange, blue and purple dashed lines, respectively.

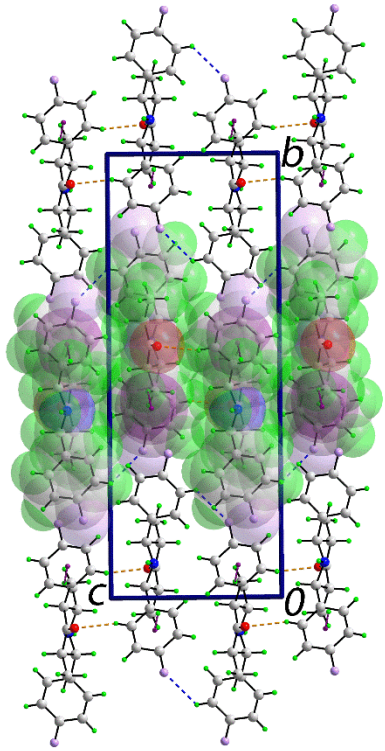

Fig. 8. A view in projection down the a-axis of the unit cell contents for **1** (unsolvated). The aryl-C–H···O(carbonyl), aryl-C–H···F and methyl-C–H···π(aryl) (largely obscured) interactions are shown as orange, blue and purple dashed lines, respectively. One layer is highlighted in space filling mode.

The crystal packing indices (packing efficiency) were calculated [32] for **1**.MeOH and **1**, and were 69.8 and 66.3%, respectively. Clearly, the inclusion of the solvent methanol molecules in **1**.MeOH reduces the amount of free space in the crystal structure. It is noteworthy that crystals of **1** were obtained from its ethanol solution [11]. This might imply that the volume increase from a methanol to an ethanol molecule cannot be accommodated efficiently in the hypothetical crystal structure of **1**.EtOH.

Hirshfeld surface analysis of 1 in the methanol solvate and unsolvated forms

Hirshfeld surface analysis provides a facile way of obtaining information about the presence of intermolecular interactions operating in the molecular packing of a given structure. The interactions within crystal structures can be used to identify the similarities and differences between closely related structures, e.g. polymorphs. The interactions can be conveniently quantified by inspecting the Hirshfeld surfaces and 2D-fingerprint (FP) plots [39]. The donors and acceptors can be highlighted similarly by mapping the Hirshfeld surfaces with d_{norm}. The Hirshfeld surfaces mapped with d_{norm}, d_e and electrostatic potential, and the 2D fingerprint plots presented herein for **1**.MeOH and **1** (unsolvated) were generated using Crystal Explorer [40].

The comparison of Hirshfeld surfaces computed for the **1**.MeOH and **1** (unsolvated) successfully explain the role of the bridging methanol molecules, through conventional hydrogen bonds, in the former. The different shapes of Hirshfeld surfaces mapped with d_{norm} for **1**.MeOH and **1**, Fig. 9, are clear indications of the presence of different type of intermolecular interactions operating in their respective crystal structures. The bright-red spots, used to predict donor and acceptor atoms in the structures, are located at different atoms in the structures thereby identifying the contribution of different intermolecular interactions.

The bright-red spots near amine-N1 and methanol-O2 on the Hirshfeld surface calculated for **1**.MeOH, Fig. 9a, is the result of potential O–H···N, N–H···O and C–H···O intermolecular interactions, each involving the methanol-O atom. The appearance of a faint red-spot at the symmetry related C35 atoms, with a 1.4 % contribution to the overall Hirshfeld surface of **1**.MeOH, also show the presence of short interatomic C35···C35 contact between layers, as mentioned above.

The faint-red spots observed at the carbonyl-O1 and F1 atoms on the Hirshfeld surface of **1**, Fig. 9b, are due to the presence intermolecular C–H···O and C–H···F interactions. The faint-red spots on the surface near aryl hydrogen atoms and the benzene ring also indicates the presence of the C–H···π interaction.

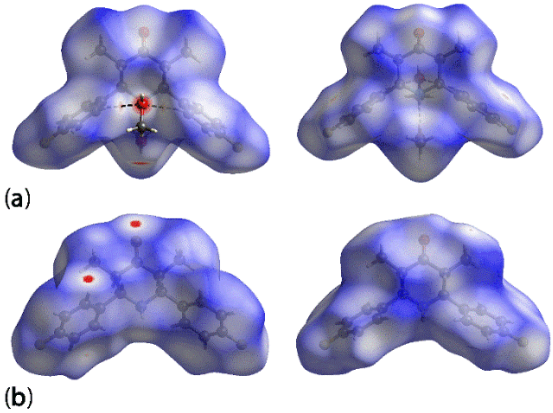

Fig. 9. Two views each of the Hirshfeld surfaces mapped over d_{norm} for (a) **1**.MeOH, and (b) **1** (unsolvated), highlighting the locations where significant intermolecular interactions are apparent.

The overall FP plots corresponding to the percentage contributions from various non-bonded contacts are shown in Fig. 10, and the breakdown FP plots for the H···H, O···H/H···O, F···H/H···F and C···H/H···C interactions are shown in Fig. 11. In addition, the FP plots delineated into F···F contacts for **1**.MeOH, and N···H/H···N contacts for **1** (unsolvated) are included in Fig. 12.

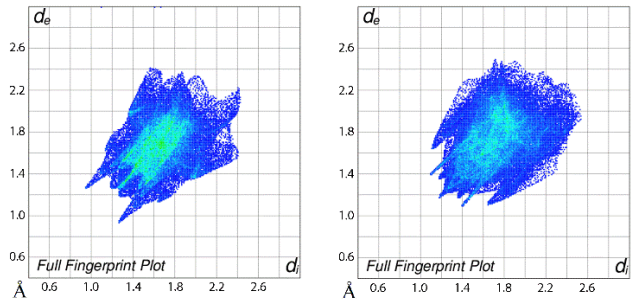

Fig. 10. Full 2D-fingerprint plots for (left-hand) **1**.MeOH, and (right-hand) **1**.

The FP plot of **1**.MeOH corresponding to O···H/H···O contacts, with a separation $d_i + d_e \sim 2.1$ Å and a pair of superimposed spikes with an overall 13.7 % contribution to the surface indicate the involvement of methanol-oxygen in hydrogen bonding interactions. Specifically, the green points with the spikes at $d_i + d_e \sim 2.7$ Å correspond to intermolecular aryl-C–H···O(methanol) interactions and the region containing blue points, having spikes at $d_i + d_e \sim 2.2$ Å, is due to the amine-N–H···O(methanol) hydrogen bonds. The intermolecular methanol-O–H···N(amine) hydrogen bond is viewed as a sharp spike $d_i + d_e \sim 1.9$ Å in the FP plot corresponding to N···H/H···N contacts. The corresponding FP plot delineated into O···H/H···O contacts for **1** shows a pair of comparatively sharp and long spikes, with $d_i + d_e \sim 2.3$ Å and an 8.5 % contribution, arising from the presence of intermolecular C–H···O interactions.

The pair of spikes observed in the FP plots delineated into F···H/H···F contacts for **1**.MeOH and **1** with respective spikes at $d_i + d_e \sim 2.8$ Å and 2.6 Å, Fig. 12, show a similar influence of non-bonded F···H/H···F contacts on the molecular packing.

The C···H/H···C interatomic contacts in the structure of **1** have, comparatively, a greater contribution to Hirshfeld surface than in **1**.MeOH with the respective values being 16.8 % and 14.1 %. The appearance in the FP plots of a thin edge for **1**.MeOH, and a broad wing for **1**, together with above quantitative values, confirm the presence of more interactions involving C···H/H···C contacts in **1** compared with **1**.MeOH. Finally, the H···H contacts, i.e. dispersive contacts, have the highest percentage contribution to the Hirshfeld surface area in each crystal structure with values of 48.2 and 50.9 % for **1**.MeOH and **1**, respectively, indicating a slightly greater contribution of H···H interatomic contacts in **1** cf. **1**.MeOH. The crystal structure of **1**.MeOH features H···H

contacts with $d_i = d_e = 1.3$ Å whereas in **1**, $d_i = d_e = 1.2$ Å. The presence of a single spike in the FP plot of **1** is due to a short interatomic H···H contact (H2···H2 = 2.36 Å; symmetry operation 1-x, -y, 1-z) and also confirms a slightly greater contribution of H···H interatomic contacts in **1**. The H···H contacts in **1**.MeOH arise as a result of a head on approach while in **1**, these are more or less due to a side-ways approach. Finally, a small contribution to the Hirshfeld surface of **1**, i.e. 2.7%, is made by weak F···F contacts beyond the sum of the van der Waals radii of fluoride as manifested in the arrowhead in Fig. 12; no such contacts were noted for **1**.MeOH.

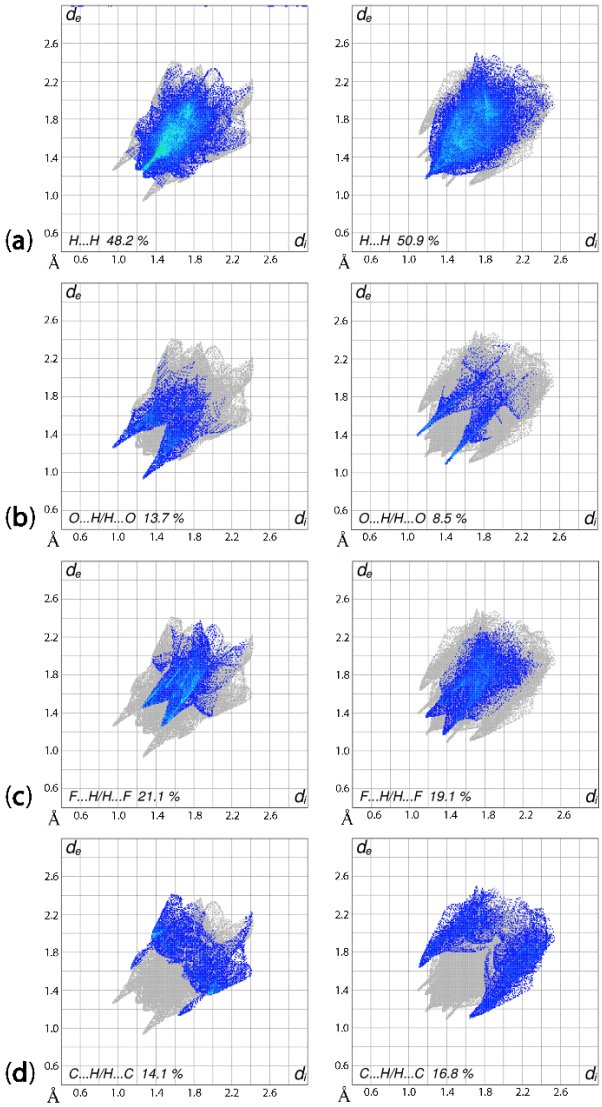

Fig. 11. A comparison of 2D-fingerprint plots for **1**.MeOH (left-hand column) and **1** (right-hand column) delineated to show (**a**) H···H, (**b**) O···H/H···O, (**c**) F···H/H···F and (**d**) C···H/H···C interactions.

The relative contributions of various intermolecular contacts to the Hirshfeld surface area in **1**.MeOH and **1** is represented graphically in Fig. 13. From this, it is evident

that despite the presence of different modes of supramolecular association in the two structures, to a first approximation, the relative contributions are the same.

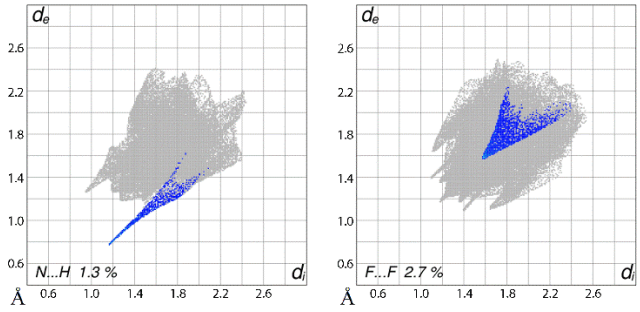

Fig. 12. 2D-fingerprint plots for **1**.MeOH (left-hand column) and **1** (right-hand column) delineated to show (**a**) N···H/H···N and (**b**) F···F interactions, respectively.

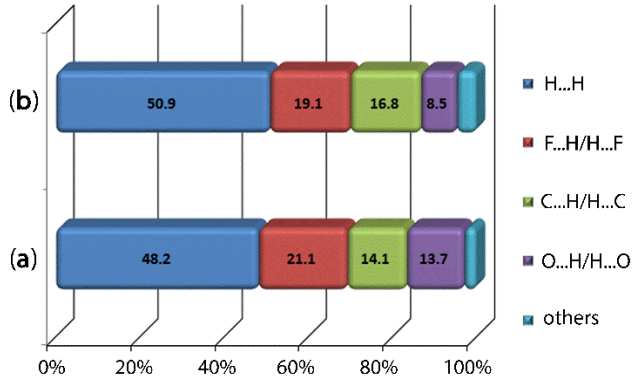

Fig. 13. Relative contributions of various intermolecular contacts to the Hirshfeld surface area in (a) **1**.MeOH and (b) **1**.

Conclusions

The molecular structure of the title 2,6-diaryl 4-piperidone derivative has been determined as its 1:1 methanol solvate, **1**.MeOH, and compared to a previously described unsolvated form, **1**, obtained from its ethanol solution [11], as well as the equilibrium structure calculated using density-functional theory (DFT). While the molecular conformations in the experimental and theoretical structures are similar, some flexibility in the relative orientations of the aryl rings is apparent. Amine-N–H···O(carbony) hydrogen bonds are not observed in either crystal structure, most likely owing to steric hindrance. The presence of solvated methanol in **1**.MeOH enables the formation of bridges between molecules via hydroxyl-O–H···N(amine) and amine-N–H···O(methanol) hydrogen bonding. Presumably, despite the conformational flexibility in the molecule, a larger ethanol molecule cannot be accommodated in a putative crystal structure of **1**.EtOH as this would result in less efficient molecular packing. An analysis of the Hirshfeld surfaces in **1**.MeOH and **1** showed

that to a first approximation, similar contributions to the surfaces by the various interactions are apparent with the greatest difference seen in the relative contributions by O···H/H···O, i.e. 13.7% in **1**.MeOH and 8.5% in **1**, reflecting the conventional hydrogen bonding in the former.

Acknowledgments. The VIT University is thanked for providing facilities. The authors also grateful to SIF-Chemistry, VIT University, for providing the NMR and X-ray diffractometer (PXRD) facilities. AOR thanks the Spanish Malta/Consolider initiative (no. CSD2007-00045) and Alberta Innovates Technology Futures (AITF) for funding. The authors also express their gratitude to the anonymous reviewers, specifically for their suggestion to re-evaluate the literature structure.

References

[1] G. R. Desiraju, Crystal Engineering: The Design of Organic Solids, Elsevier, Amsterdam, **1989**.
[2] M. C. Etter, *Acc. Chem. Res*. **1990**, *23*, 120.
[3] G. R. Desiraju and T. Steiner, The Weak Hydrogen Bond in Structural Chemistry and Biology, Oxford University Press, Oxford, **1999**.
[4] G. R. Desiraju, *J. Am. Chem. Soc*. **2013**, *135*, 9952.
[5] T. Shattock, K. K. Arora, P. Vishweshwar, M. J. Zaworotko, *Cryst. Growth Des*. **2008**, *8*, 4533.
[6] C. Aakeröy, *Acta Crystallogr. B*, **2015**, *71*, 387.
[7] W. Bolton, *Acta Crystallogr*. **1964**, *17*, 147.
[8] F. H. Allen, C. A. Baalham, J. P. M. Lommerse, and P. R. Raithby, *Acta Crystallogr*. *B*, **1998**, *54*, 320.
[9] M. V. Câmpion, I. Haiduc, E. R. T. Tiekink, *Z. Kristallogr*. – *Cryst. Mat*. **2013**, *228*, 187.
[10] J. D. Dunitz, W. B. Schweizer, *CrystEngComm*, **2007**, *9*, 266.
[11] D. Gayathri, D. Velmurugan, G. Aridoss, S. Kabilan, K. Ravikumar, *Acta Cryst. E*, **2008**, *64*, o429.
[12] C. Ramalingam, Y. T. Park, S. Kabilan, *Eur. J. Med. Chem.* **2006**, *41*, 683.
[13] G. Aridoss, S. Amirthaganesan, Y. Y. Jeong, *Bioorg. Med. Chem Lett*. **2010**, *20*, 2242.
[14] N. Rameshkumar, A. Veena, R. Ilavarasan, M. Adiraj, P. Shanmugapandiyan, S. K. Sridhar, *Biol. Pharm. Bull*. **2003**, *26*, 188.
[15] S. Balasubramanian, G. Aridoss, P. Parthiban, C. Ramalingam, S. Kabilan, *Biol. Pharm. Bull*. **2006**, *29*, 125.
[16] G. Aridoss, S. Amirthaganesan, N. Ashok Kumar, J. T. Kim, K. T. Lim, S. Kabilan, Y. T. Jeong, *Bioorg. Med. Chem. Lett*. **2008**, *18*, 6542.
[17] B. Ileana, V. Dobre, I. Niculescu-Duvaz, *J. Prakt. Chem.* **1985**, *327*, 667.
[18] M. Bazzaro, K. A. Ravi, R. M. Mohana Krishna, O. Issaenko, S. Kumar, B. Karanam, Z. Lin, R. I. Vogel, R. Gavioli, F. Destro, V. Ferretti, R. B. S. Roden, S. R. Khan, *J. Med. Chem.* **2011**, *54*, 449.
[19] S. Rastigi, H. Rastogi, *Indian J. Chem*. **2010**, *49*, 547.
[20] I. G. Mobio, A. T. Soldatenkov , V. O. Fedrov, E. A. Ageev, N. D. Sergeeva, S. Lin, E. E. Stashenko, N. S. Prostakov, E. I. Andreeva, *Khim. Farm. Zh*. **1989**, *23*, 421.

[21] A. Casy, J. Coates, C. Rostron, *J. Pharm. Pharmacol*. **1976**, *28*, 106.
[22] V. Vijayakumar, M. Sundaravadivelu, S. Perumal, *Mag. Reson. Chem*. **2001**, *39*, 101.
[23] G. L. Balaji, V. Vijayakumar, K. Rajesh, *Arab. J. Chem.* **2012**, doi:10.1016/j.arabjc.2011.12.011.
[24] K. Rajesh, B. Palakshi Reddy, V. Vijayakumar, *Ultrason. Sonochem*. **2012**, *19*, 522.
[25] N. Kourkoumelis, PowDLL. ICDD Annual Spring Meetings (Ed. Lisa O'Neill), Powder Diffraction, 28 (2013) 137-148.
[26] X'Pert HighScore Plus. PANalytical B.V. Almelo, The Netherlands, **2009**.
[27] C. R. Noller, V. Baliah, *J. Am. Chem. Soc*. **1948**, *70*, 3853.
[28] Agilent Technologies, *CrysAlisPro*. Santa Clara, CA, USA. **2014**.
[29] G. M. Sheldrick, *Acta Crystallogr. A* **2008**, *64*, 112.
[30] G. M. Sheldrick, *Acta Crystallogr. C* **2015**, *71*, 3.
[31] L. J. Farrugia, *J. Appl. Crystallogr*. **2012**, *45*, 849.
[32] A. L. Spek, *Acta Crystallogr. D* **2009**, *65*, 148.
[33] J. Gans, D. Shalloway, *J. Mol. Graph. Model*. **2001**, *19*, 557.
[34] DIAMOND, Visual Crystal Structure Information System, Version 3.1, CRYSTAL IMPACT, Postfach 1251, D-53002, **2006**.
[35] M. J. Frisch, G. W. Trucks, H. B. Schlegel, G. E. Scuseria, M. A. Robb, J. R. Cheeseman, G. Scalmani, V. Barone, B. Mennucci, G. A. Petersson, H. Nakatsuji, M. Caricato, X. Li, H. P. Hratchian, A. F. Izmaylov, J. Bloino, G. Zheng, J. L. Sonnenberg, M. Hada, M. Ehara, K. Toyota, R. Fukuda, J. Hasegawa, M. Ishida, T. Nakajima, Y. Honda, O. Kitao, H. Nakai, T. Vreven, J. A. Montgomery Jr., J. E. Peralta, F. Ogliaro, M. J. Bearpark, J. Heyd, E. N. Brothers, K. N. Kudin, V. N. Staroverov, R. Kobayashi, J. Normand, K. Raghavachari, A. P. Rendell, J. C. Burant, S. S. Iyengar, J. Tomasi, M. Cossi, N. Rega, N. J. Millam, M. Klene, J. E. Knox, J. B. Cross, V. Bakken, C. Adamo, J. Jaramillo, R. Gomperts, R. E. Stratmann, O. Yazyev, A. J. Austin, R. Cammi, C. Pomelli, J. W. Ochterski, R. L. Martin, K. Morokuma, V. G. Zakrzewski, G. A. Voth, P. Salvador, J. J. Dannenberg, S. Dapprich, A. D. Daniels, Ö. Farkas, J. B. Foresman, J. V. Ortiz, J. Cioslowski and D. J. Fox, Gaussian 09, Revision A.1, Gaussian, Inc., Wallingford, CT, USA, **2009**.
[36] A. D. Becke, *J. Chem. Phys*. **1993**, *98*, 5648.
[37] C. Lee, W. Yang, R. G. Parr, *Phys. Rev. B* **1988**, *37*, 785.
[38] AIMAll (Version 16.01.09), Todd A. Keith, TK Gristmill Software, Overland Park KS, USA, **2016**.
[39] A. L. Rohl, M. Moret, W. Kaminsky, K. Claborn, J. J. Mackinnon, B. Kahr, *Cryst. Growth Des*. **2008**, *8*, 4517.
[40] S. K. Wolff, D. J. Grimwood, J. J. McKinnon, M. J. Turner, D. Jayatilaka, M. A. Spackman, Crystal Explorer (Version 3.1), University of Western Australia, **2012**.

Hydrogen bonding in 2,6-bis(4-fluorophenyl)-3,5-dimethylpiperidin-4-one methanol solvate

T. Suresh,[I,II] V. Vijayakumar,[I] L. Jyothish Kumar,[I] S. Sarveswari*[I], Mukesh M. Jotani,[III] A. Otero-de-la-Roza,[IV] Yee Seng Tan[V] and Edward R. T. Tiekink*[V]

[I] VIT University, Centre for Organic and Medicinal Chemistry, Vellore, Tamil Nadu 632014, India

[II] Orchid Chemicals & Pharmaceuticals Ltd, R&D Centre, Chennai 600119, India

[III] Bhavan's Sheth R. A. College of Science, Department of Physics, Ahmedabad, Gujarat 380001, India

[IV] National Research Council of Canada, National Institute for Nanotechnology, 11421 Saskatchewan Drive, Edmonton, Alberta,

Canada T6G 2M9

[V] Sunway University, Research Centre for Crystalline Materials, Faculty of Science and Technology, 47500 Bandar Sunway, Selangor Darul Ehsan, Malaysia

***** SUPPLEMENTARY MATERIAL *****

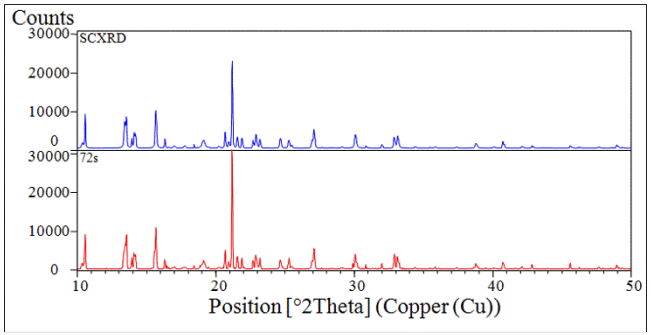

Figure S1. Experimental (red trace) and simulated based on the single crystal structure (blue trace) PXRD patterns for **1**.MeOH. These show that the single crystal data reported herein for **1**.MeOH match the structure of the bulk material.